Eur. Phys. J. B **23**, 153–158 (2001)

THE EUROPEAN PHYSICAL JOURNAL B

EDP Sciences

Magnetic properties of undoped $YBa_2Cu_3O_{6+x}$ system

Govind[1,a], A. Pratap[1], Ajay[2], and R.S. Tripathi[2]

[1] Theory Group, National Physical Laboratory, Dr. K.S. Krishnan Marg, New Delhi 110012, India
[2] Department of Physics, G.B. Pant University of Ag. & Tech. Pantnagar 263145, India

Received 13 July 2000 and Received in final form 14 May 2001

Abstract. In the present paper, we study the magnetic properties of bilayer cuprate antiferromagnets. In order to evaluate the expressions for spin-wave dispersion, sublattice magnetization, Néel temperature and the magnetic contribution to the specific heat, the double time Green's function technique has been employed in the random phase approximation (RPA). The spin wave dispersion curve for a bilayer antiferromagnetic system is found to consist of one acoustic and one optic branch. The "optical magnon gap" has been attributed solely to the intra-bilayer exchange coupling ($J_\perp$) as its magnitude does not change significantly with the inter-bilayer exchange coupling (J_z). However J_z is essential to obtain the acoustic mode contribution to the magnetization. The numerical calculations show that the Néel temperature (T_N) of the bilayer antiferromagnetic system increases with the J_z and a small change in J_z gives rise to a large change in the Néel temperature of the system. The magnetic specific heat of the system follows a T^2 behaviour but in the presence of J_z it varies faster than T^2.

PACS. 75.30.-m Intrinsic properties of magnetically ordered materials – 74.72.Bk Y-based cuprates – 75.10.Jm Quantized spin models

1 Introduction

In the undoped state, the cuprate superconductors like La_2CuO_4, and $YBa_2Cu_3O_6$ (123) are layered antiferromagnetic (AFM) insulators. Due to their layered structure these systems possess anisotropy in many of their physical properties. The La_2CuO_4 system has only one CuO_2 plane per unit cell. The magnetic properties in the insulating phase of this material can be well described by the Heisenberg model with in-plane AFM exchange coupling ($J_\parallel$) and inter unit cell exchange coupling (J_z) [1–8]. On the other hand, $YBa_2Cu_3O_6$ has two layers per unit cell and the electronic states of these CuO_2 layers are strongly coupled right from the undoped to overdoped phase [9–13]. Therefore unlike single layered La_2CuO_4 system the study of magnetic dynamics of bilayer system requires extra attention.

It has been observed in $YBa_2Cu_3O_{6+x}$, that the intra-bilayer coupling ($J_\perp$) leads towards the presence of an acoustic and an optic mode in the magnon dispersion and a magnon gap of the order of 65–70 meV [14]. It has also been observed [15] that inter-bilayer exchange coupling (J_z) is important to establish long range order (3D Néel ordering) in these systems and plays a significant role in the magnetic dynamics.

Several theoretical efforts have been made to investigate the normal state magnetic properties of cuprate systems. These calculations mainly deal with the single layer and two-sublattice models within the random phase approximation [1,2], spin-waves [3], the Callen decoupling scheme [4] and the Schwinger boson approach [6,7]. By contrast, to date, theoretical studies for the bilayer cuprates have been performed by considering the in-plane and the intra-bilayer exchange coupling only. Millis *et al.* [16,17] have calculated the dynamical susceptibility of these systems within the Schwinger boson technique. They estimated that the intra-bilayer exchange coupling strength ($J_\perp$) is about 14 meV. Du *et al.* [18] have shown that in the absence of intra- or inter- bilayer exchange coupling the system does not show long range magnetic order and the Néel temperature vanishes.

More recently, we have discussed the magnetic dynamics of a bilayer antiferromagnetic system ($YBa_2Cu_3O_{6+x}$) within linear spin wave approximation [15]. In this study, we consider in-plane and intra-bilayer exchange coupling in the model Hamiltonian while the role of inter-bilayer exchange coupling was introduced phenomenologically. We have examined the role of the optic and acoustic magnetic excitations on the magnetic dynamics of bilayer systems and found that in the absence of anisotropy, the acoustic mode may not sustain magnetization.

In view of this, in the present paper, we incorporate the effects of inter-bilayer exchange coupling explicitly into the microscopic model Hamiltonian and plan to study its role on the magnetic properties of bilayer cuprates. We employ Green's function formalism [19] for a four sublattice model within the random phase approximation and

[a] e-mail: govind@csnpl.ren.nic.in

$$H = J_{\parallel} \sum_{i\neq j,\alpha\neq\beta} [S_{ia\alpha}S_{jb\alpha} + S_{ja\alpha}S_{ib\alpha} + S_{ic\alpha}S_{jd\alpha} + S_{jc\alpha}S_{id\alpha}]$$
$$+ J_{\perp} \sum_{i,\alpha\neq\beta} [S_{ia\alpha}S_{ic\beta} + S_{ia\beta}S_{ic\alpha} + S_{ib\alpha}S_{id\beta} + S_{ib\beta}S_{id\alpha}]$$
$$+ J_z \sum_{\substack{i,\alpha\neq\beta \\ \delta'}} [S_{ia\alpha}S_{i+\delta' c\beta} + S_{ia\beta}S_{i+\delta' c\alpha} + S_{ib\alpha}S_{i+\delta' d\beta} + S_{ib\beta}S_{i+\delta' d\alpha}],$$

obtain expressions for sublattice magnetization, Néel temperature and magnetic specific heat for bilayer antiferromagnets. We organize the paper in the following way. The theoretical formulation is presented in Section 2. Expressions for staggered magnetization, Néel temperature and magnetic specific heat are presented in Sections 3, 4, 5 respectively. The numerical results and discussions are given in Section 6.

2 Theoretical formulation

For bilayer systems, we define the Heisenberg antiferromagnetic Hamiltonian as:

$$H = J_{\perp} \sum_{i,j,\alpha} S_{i\alpha}S_{j\alpha} + J_{\perp} \sum_{i,\alpha} S_{i\alpha}S_{i\beta} + J_z \sum_{i,\delta'} S_{i\alpha}S_{i+\delta'\beta}. \tag{1}$$

In four sublattice model the above Hamiltonian can be explicitly written as

see equation above

where, $\alpha\beta = 1(2)$ are the layer indices, i, j denotes the lattice sites with j is the nearest neighbour of i, δ is the nearest neighbour distance within plane and δ' is the distance between the two bilayers. The suffixes a, b, c and d denote the four sublattices of the system. $J_{\parallel}$ is the in-plane exchange coupling and $J_{\perp}$, J_z are intra- and inter-bilayer exchange couplings respectively. A figure describing various exchange couplings for a bilayer system with four basis atoms (a, b, c, and d) is shown in Figure 1. We define for this purpose the following Green's functions

$$G_1 = \langle\langle S^+_{ia1}; S^-_{ia1}\rangle\rangle \quad G_2 = \langle\langle S^+_{ib1}; S^-_{ia1}\rangle\rangle$$
$$G_3 = \langle\langle S^+_{ic2}; S^-_{ia1}\rangle\rangle \quad G_4 = \langle\langle S^+_{id2}; S^-_{ia1}\rangle\rangle \tag{2}$$

where $S^{\pm} = S^x \pm \mathrm{i}S^y$ are the spin raising and lowering operators. The equation of motion for the Green's function $\langle\langle S^+_{ia1}; S^-_{ia1}\rangle\rangle$ can be written as

$$\omega G_1 = \frac{1}{2\pi}\left\langle \left[S^+_{ia1}; S^-_{ia1}\right] \right\rangle + \left\langle\left\langle [S^+_{ia1}, H]; S^-_{ia1}\right\rangle\right\rangle \cdot \tag{3}$$

Further, to solve the commutator shown in equation (3), we use the following commutation rules

$$\left[S^z_{\mathrm{ln}\alpha}; S^{\pm}_{l'n'\alpha'}\right] = \pm\delta_{\alpha\alpha'}\delta_{ll'}\delta_{nn'}S^{\pm}_{\mathrm{ln}\alpha}$$

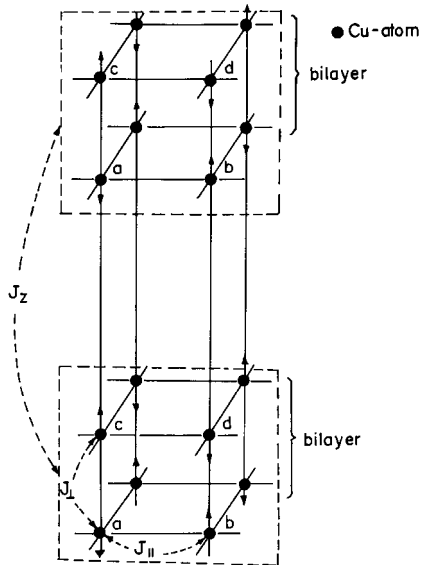

Fig. 1. A four sublattice model (a,b,c,d) of bilayer cuprates with $J_{\parallel}$ (in-plane exchange coupling), $J_{\perp}$ (intra-bilayer coupling) and J_z (inter-bilayer exchange coupling).

and

$$\left[S^+_{\mathrm{ln}\alpha}; S^-_{l'n'\alpha'}\right] = \delta_{\alpha\alpha'}\delta_{ll'}\delta_{nn'}(2S^z_{\mathrm{ln}\alpha}) \tag{4}$$

where, $l(l')$ denote the lattice site, $n(n')$ denotes the sublattices and $\alpha(\alpha')$ denotes the layer indices. We decouple the equation (3) within the random phase approximation using the following procedure

$$\langle\langle S^z_{\mathrm{ln}\alpha}S^{\pm}_{l'n'\alpha'}; S^-_{ia\beta}\rangle\rangle = \langle S^z_{\mathrm{ln}\alpha}\rangle\langle\langle S^{\pm}_{l'n'\alpha'}; S^-_{ia\beta}\rangle\rangle \cdot \tag{5}$$

The symmetry of the system allows

$$\langle S^z_{ia1}\rangle = \langle S^z_{id2}\rangle = -\langle S^z_{ib1}\rangle = -\langle S^z_{ic2}\rangle = \bar{S}. \tag{6}$$

We solve equation (3) using (4–6). Finally, we are left with four coupled equations corresponding to various Green's function. These can be presented in the form of a matrix:

$$\begin{bmatrix} \omega-\varepsilon & -J_1(k) & -J_2(k) & 0 \\ J_1(k) & \omega+\varepsilon & 0 & J_2(k) \\ J_2(k) & 0 & \omega+\varepsilon & J_1(k) \\ 0 & -J_2(k) & -J_1(k) & \omega-\varepsilon \end{bmatrix} \begin{bmatrix} G_1 \\ G_2 \\ G_3 \\ G_4 \end{bmatrix} = \begin{bmatrix} 1/2\pi \\ 0 \\ 0 \\ 0 \end{bmatrix} \tag{7}$$

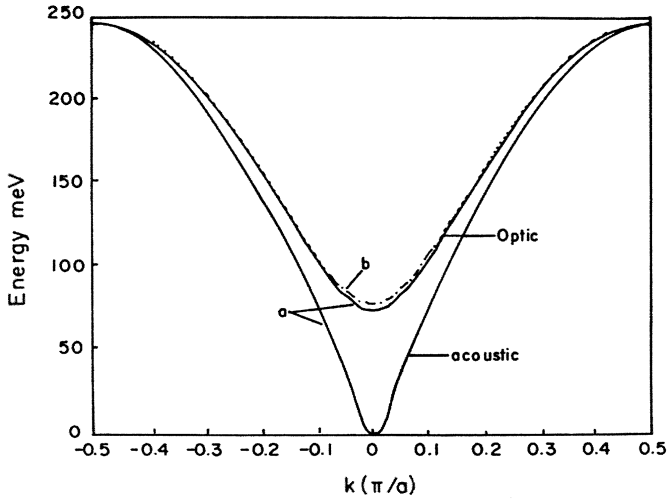

Fig. 2. Dispersion energy (ω) with wave vector k ($k_x = k_y$) and small value of $k_z c$ with (a) $R = 1 \times 10^{-5}$ and (b) $R = 5 \times 10^{-3}$ for $J_\parallel = 120$ meV and $r = 0.1$.

where

$$J_1(k) = 2J_\parallel \bar{S} Z_{ab} \gamma_\parallel(k)$$
$$J_2(k) = 2J_\perp \bar{S} + 2J_z \bar{S} Z_c \gamma_c(k)$$
$$\varepsilon = 2J_\parallel \bar{S} Z_{ab} + 2J_\perp \bar{S} + 2J_z \bar{S} Z_c.$$

with $\gamma_\parallel(k) = \frac{1}{Z_{ab}} \sum_\delta^{ab} \exp(\mathrm{i}k\delta)$, $\gamma_c(k) = \frac{1}{Z_c} \sum_{\delta'}^{c} \exp(\mathrm{i}k\delta')$. $Z_{ab} = 4$ and $Z_c = 2$ are the nearest neighbour in the ab-plane and in the c-direction. The solution of equation (7) gives

$$\omega_{1,2k}^2 = \left(\varepsilon^2 - \left[J_1(k) \pm J_2(k)\right]^2\right). \tag{8}$$

Substituting the values of $J_1(k)$ and $J_2(k)$, we obtain

$$\omega_{1,2k} = 2J_\parallel \bar{S} \Big[(4 + r + 2R)^2 - \left\{2(\cos k_x a + \cos k_y a) \pm (r + 2R \cos k_z c)\right\}^2\Big]^{1/2}, \tag{9}$$

with $r = J_\perp / J_\parallel$, $R = J_z / J_\parallel$.

Here, the (+) sign corresponds to the acoustic while the (−) sign corresponds to the optic mode in the excitation spectrum. In Figure 2, we have plotted the dispersion energies of the acoustic and optic modes for $k_x = k_y = k(-\pi/2a$ to $\pi/2a)$ for different values of inter-bilayer exchange coupling. The magnitude of the calculated magnon gap is ≈75 meV which is very close to the previously obtained values (65−70 meV) [13–18]. The expression for the magnon gap is modified due to the contribution of J_z and reads $E_g = 8\bar{S}\sqrt{J_\parallel (J_\perp + 2J_z)}$. We solve the set of equations (7) and obtain Green's function relevant to the magnetic properties given by

$$G_1 = \frac{\bar{S}}{2\pi} \sum_k \left[\frac{(\omega + \varepsilon)}{(\omega^2 - \omega_{1k}^2)} + \frac{(\omega + \varepsilon)}{(\omega^2 - \omega_{2k}^2)}\right]. \tag{10}$$

Following the standard procedure of Zubarev [19], we obtain the correlation function $\langle S^- S^+ \rangle$ for the Green's function in equation (10) which may be written as

$$\langle S^- S^+ \rangle = \frac{\bar{S}}{N} \sum_k \left[\frac{\varepsilon}{2\omega_{1k}} \coth(\beta_{\omega_{1k}}/2) + \frac{\varepsilon}{2\omega_{2k}} \coth(\beta_{\omega_{2k}}/2) - 1\right]. \tag{11}$$

3 Staggered magnetization

In this section, we calculate magnetization of a bilayer antiferromagnetic system. The magnetization may be evaluated by using the relation

$$\langle S^z \rangle = \frac{1}{2} - \langle S^- S^+ \rangle \tag{12}$$

where the correlation $\langle S^- S^+ \rangle$ is given by equation (11) and $\langle S^z \rangle$ gives the magnetization at temperature T which reads

$$M(T) = \frac{1}{2} - \frac{\bar{S}}{N} \sum_k \left[\frac{\varepsilon}{2\omega_{1k}} \coth(\beta_{\omega_{1k}}/2) + \frac{\varepsilon}{2\omega_{2k}} \coth(\beta_{\omega_{2k}}/2) - 1\right]. \tag{13}$$

We first consider the zero temperature correction to the sublattice magnetization due to spin quantum fluctuations. From equation (13) this comes out to be

$$M(0) = \frac{1}{2} - \frac{\bar{S}}{N} \sum_k \left[\frac{\varepsilon}{2\omega_{1k}} + \frac{\varepsilon}{2\omega_{2k}} - 1\right]. \tag{14}$$

If in the above equations (13) and (14), we set $\bar{S} = 1/2$ and the inter-bilayer exchange coupling $J_z = 0$, this reduces to our previous results [15] of the spin wave approximation. Furthermore, the expression for staggered magnetization is obtained from (13) and is given by

$$-\delta M(T) = M(T) - M(0) = -\frac{\bar{S}}{N} \times \sum_k \left[\frac{\varepsilon}{\omega_{1k}\left(\exp(\beta_{\omega_{1k}}) - 1\right)} + \frac{\varepsilon}{\omega_{2k}\left(\exp(\beta_{\omega_{2k}}) - 1\right)}\right]. \tag{15}$$

For very small values of intra- (r) and inter-bilayer (R) exchange coupling ratio, the leading contribution to the magnetization comes from the small k-values [2] and under such condition we can approximate $\cos k_x a = 1 - (k_x a)^2/2$, $\cos k_y a = 1 - (k_y a)^2/2$. Further, we denote $(k_x a)^2 + (k_y a)^2 = \theta_p^2$ and $k_z c = \theta_z$, and replace the summation over k-values by an integration. We finally obtain

$$\delta M = \frac{(4 + r + 2R)\bar{S}}{2\pi^2} \left[\int_{-\pi}^{\pi} \mathrm{d}\theta_z \int_0^\infty \frac{\theta_p \mathrm{d}\theta_p}{\omega_{1k}\left(\exp(\beta_{\omega_{1k}}) - 1\right)} + \int_{-\pi}^{\pi} \mathrm{d}\theta_z \int_0^\infty \frac{\theta_p \mathrm{d}\theta_p}{\omega_{2k}\left(\exp(\beta_{\omega_{2k}}) - 1\right)}\right]. \tag{16}$$

$$I_1(\omega) = \frac{\left[(\ln R^{1/2} - 1) - \left(\frac{\ln(8+2r+3R)}{2} - 1\right) - \left\{\frac{(8+2r+4R)^{1/2}}{2R^{1/2}} \ln\left|\frac{R^{1/2}+(8+2r+4R)^{1/2}}{R^{1/2}-(8+2r+4R)^{1/2}}\right|\right\}\right]}{(4+r+2R)(4\pi^2)} \tag{20}$$

$$I_2(\omega) = \frac{\left[\left\{2 - \frac{\ln(2r+4R+8)}{2} + \left(\sqrt{8R}\right)\tan^{-1}\left(\frac{R^{1/2}}{2\sqrt{2}}\right)\right\} - \left\{\frac{(2r+4R)^{1/2}}{2R^{1/2}} \ln\left|\frac{R^{1/2}+(2r+4R)^{1/2}}{R^{1/2}-(2r+4R)^{1/2}}\right|\right\}\right]}{(4+r+2R)(4\pi^2)}\,. \tag{21}$$

We solve the above equation self consistently and calculate the value of sublattice magnetization.

4 Néel temperature

The Néel temperature is obtained from equation (13) under the condition $T \to T_{\rm N}$; $M(T) \to 0$. Thus the Néel temperature is given by

$$T_{\rm N} = \frac{1}{k_{\rm B}}\left[\frac{J_{\parallel}}{(4+r+2R)I_{12}(\omega)}\right] \tag{17}$$

with
$$I_{12}(\omega) = \frac{1}{N}\sum_k \left(\frac{1}{\omega_{1k}^2} + \frac{1}{\omega_{2k}^2}\right) \tag{18}$$

where $\omega_{1,2k}$ is given by (9). We solve equation (18) by converting the summation into an integration over k-values. The analytical evaluation of $I_{12}(\omega)$ may be written as

$$I_{12}(\omega) = I_1(\omega) + I_2(\omega) \tag{19}$$

with

see equations (20) and (21) above.

Substituting values of $I_{12}(\omega)$ into equation (17), we calculate the Néel temperature for a bilayer system with intra- and inter-bilayer contributions of the exchange couplings.

5 Magnetic specific heat

In this section, we obtain an expression for the magnetic contribution to the specific heat using the standard procedure,

$$C_{\rm M}(T) = \frac{\partial U}{\partial T}\,. \tag{22}$$

Here U is the internal energy of the system and at temperature T this is given by

$$U = \sum_k \left[\frac{\omega_{1k}}{(\exp(\beta_{\omega_{1k}}) - 1)} + \frac{\omega_{2k}}{(\exp(\beta_{\omega_{2k}}) - 1)}\right]. \tag{23}$$

Differentiating equation (23), with respect to temperature and substituting the values of ω_{1k} and ω_{2k} from equation (9). We get

$$C_{\rm M}(T) = C_{\rm M1}(T) + C_{\rm M2}(T) \tag{24}$$

$$C_{\rm M1}(T) = \sum_k \left[\frac{\omega_{1k}^2}{k_{\rm B}T^2}\,\frac{\exp(\omega_{1k}/k_{\rm B}T)}{[\exp(\omega_{1k}^2/k_{\rm B}T) - 1]^2}\right] \tag{25}$$

$$C_{\rm M2}(T) = \sum_k \left[\frac{\omega_{2k}^2}{k_{\rm B}T^2}\,\frac{\exp(\omega_{2k}/k_{\rm B}T)}{[\exp(\omega_{2k}^2/k_{\rm B}T) - 1]^2}\right]. \tag{26}$$

Converting the summation over k-values into an integration, the above equations (25) and (26) can be evaluated as

$$C_{\rm M1}(T) = \frac{1}{2\pi^2}\left(\frac{k_{\rm B}^2T^2}{J_{\parallel}^2\bar{S}^2}\right)\int_{-1}^{1}\theta_z\int_{\lambda 1}^{\infty}\frac{x^3 \mathrm{cosesh}^2 x \mathrm{d}x}{a} \tag{27}$$

$$C_{\rm M2}(T) = \frac{1}{2\pi^2}\left(\frac{k_{\rm B}^2T^2}{J_{\parallel}^2\bar{S}^2}\right)\int_{-1}^{1}\theta_z\int_{\lambda 2}^{\infty}\frac{x^3 \mathrm{cosesh}^2 x \mathrm{d}x}{c} \tag{28}$$

with

$$\lambda_1 = \bar{S}b^{1/2}/(2k_{\rm B}T)$$
$$\lambda_2 = \bar{S}d^{1/2}/(2k_{\rm B}T)$$

and,

$$\begin{aligned} a &= 2(4+r+2R\cos\theta_z)\\ b &= 4R^2(1-\cos^2\theta_z) + 4R(4+r)(1-\cos\theta_z)\\ c &= 2(4-r-2r\cos\theta_z)\\ d &= 16 + 4R^2(1-\cos^2\theta_z)\\ &\quad +16R(1+\cos\theta_z) + 4rR(1-\cos\theta_z). \end{aligned}$$

Here, while calculating the magnetic contribution to the specific heat at low temperatures, we have not considered the temperature dependence of $\bar{S}$. Solving these expressions numerically, we study the effect of intra- (r) and inter-bilayer (R) exchange coupling on the magnetic specific heat of a bilayer cuprates.

6 Results and discussion

We now present the numerical estimation of our expressions for the various magnetic properties *i.e.* staggered magnetization, Néel temperature and magnetic specific heat for different values of in-plane and out-of-plane

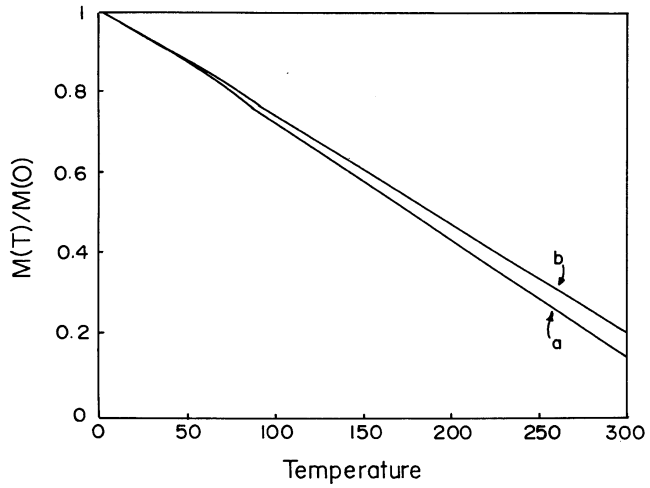

Fig. 3. Normalised magnetization ($M(T)/M(0)$) *vs.* temperature (T) for (a) $R = 1 \times 10^{-5}$ and (b) $R = 0.1$ with $J_{\|} = 120$ meV and $r = 0.1$.

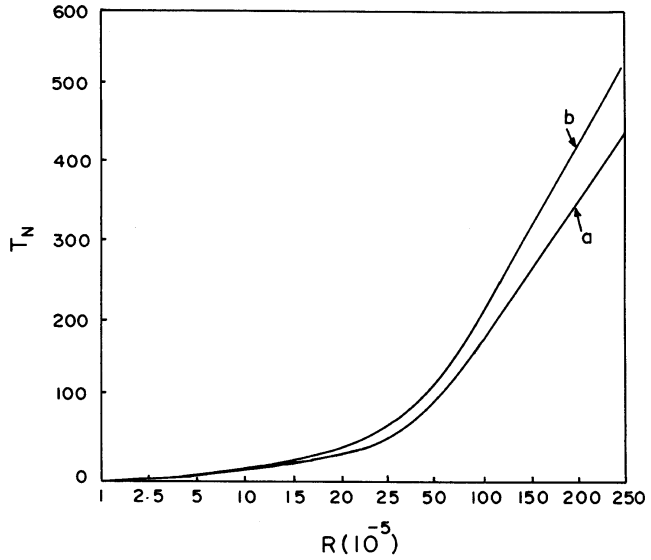

Fig. 4. Néel temperature (T_N) *vs.* inter-bilayer exchange coupling (R) for (a) $J_{\|} = 100$ meV and (b) $J_{\|} = 120$ meV with $r = 0.1$.

(intra- and inter-bilayer) antiferromagnetic exchange couplings. Following earlier works [14–16], we set the in-plane exchange coupling, $J_{\|} = 120$ meV, and the intra-bilayer exchange coupling, $J_{\perp} = 0.1J_{\|}$.

We plot reduced magnetization ($M(T)/M(0)$) *vs.* temperature for different values of the ratio of inter-bilayer exchange coupling to the in-plane coupling strength ($R = J_z/J_{\|}$) in Figure 3. It is clear from Figure 3, that on increasing the strength of inter-bilayer coupling, magnetization increases. This is in accord with the experimental observations which suggest that inter-bilayer exchange coupling (J_z) is essential to keep long range magnetic order in these systems [9–11]. It also implies that in the absence of inter-bilayer exchange coupling (J_z) these bilayers behave like a 2D-AFM system and the three-dimensional natures of AFM cuprates cannot be achieved. It is also observed that the magnetization does not change significantly with intra-bilayer exchange coupling ($J_{\perp}$).

We, next calculate the Néel temperature of these bilayer system numerically from equation (17). Dependence of the Néel temperature on the weak interlayer coupling has already been discussed [8] for single layer systems but the effect of inter-bilayer exchange coupling in the presence of intra-bilayer coupling has not been studied. Recently, we have studied the effect of intra-bilayer exchange coupling on the Néel temperature [20], where the contribution of inter-bilayer exchange coupling has been treated phenomenologically in the model Hamiltonian. Here in Figure 4, we plot Néel temperature *vs.* the ratio of inter-bilayer exchange coupling to in-plane exchange couplings (R) for $J_{\|} = 100$ meV and 120 meV, keeping the intra-bilayer coupling fixed. It is clear from Figure 4 that on increasing the strength of in-plane or inter-bilayer exchange couplings, the Néel temperature of the system increases. We conclude from the Figure 4 that any small change in inter-bilayer exchange coupling causes significant change in the Néel temperature of the system.

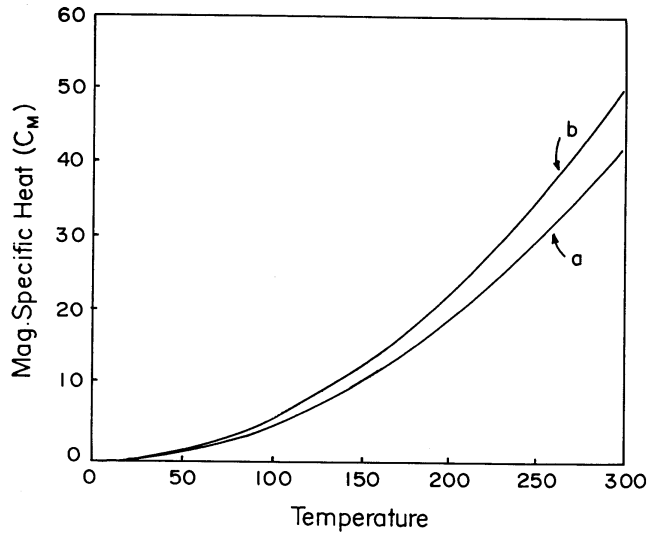

Fig. 5. Magnetic specific heat (C_M) *vs.* temperature (T) for (a) $R = 1 \times 10^{-5}$ and (b) $R = 1.0$ with $J_{\|} = 120$ meV and $r = 0.1$.

Finally, we plot magnetic specific heat of the bilayer system for various values of the exchange coupling from equation (24). The expression for specific heat clearly shows a T^2 behaviour. In Figure 5, we plot the magnetic specific heat *vs.* temperature for different values of the ratio of inter-bilayer to in-plane exchange coupling (R). It is clear from the figure that on increasing the inter-bilayer exchange coupling the magnetic contribution to specific heat increases. The magnetic specific heat shows a variation higher than T^2 as inter-bilayer exchange coupling is considerable high (*i.e.* $R = 1.0$). It is also clear from Figure 5 that at low temperatures the variation in the

magnetic specific heat due to inter-bilayer exchange coupling is very small. To calculate the magnetic contribution to the specific heat at low temperature it is important to consider the temperature dependence of magnatisation, in fact, magnetisation varies as T^2 at low temperatures but at high temperatures it follows a $T\ln T$ behaviour [6,15]. Hence it is important to study the magnetic contribution to the specific heat at low temperature by taking the temperature dependence of magnetisation into account.

It can be concluded that inter-bilayer exchange coupling (J_z) however small, is essential to keep 3D long range magnetic ordering in the system. Both the optic and acoustic spin wave modes contribute towards the long range magnetic order in the presence of inter-bilayer exchange coupling. On the other hand the magnon gap is not very sensitive to the inter-bilayer exchange coupling (J_z). This is because of the smallness of J_z in comparison to $J_\perp$. Moreover, one can infer from this that the magnon gap has nothing to do with long range magnetic order in the bilayer systems. The magnetic specific heat shows a dependence higher than T^2 as inter-bilayer exchange coupling is introduced. Thus, the present investigation based on RPA, clearly illustrates the importance of the role of J_z in the magnetic dynamics of $YBa_2Cu_3O_{6+x}$ bilayer cuprates. The bilayer cuprates behave in a quite different way to single layered La_2CuO_4 system in the insulating AF magnetic phase and it will be interesting to extend the present calculations to doped bilayer systems.

We are thankful to Prof. S.K. Joshi and Dr. R. Lal, NPL, for useful suggestions and discussions. The work is financially supported by Council of Scientific & Industrial Research, New Delhi, India, vide Grant 31/1/(180)/2000 EMR-I and Department of Science & Technology, New Delhi, India, vide Grant No. SP/S2/M-32/99.

References

1. A. Singh, Z. Tesanovic, H. Tang, G. Xiao, C.L. Chien, J.C. Walker, Phys. Rev. Lett. **64**, 2571 (1990).
2. R.P. Singh, Z.C. Tao, M. Singh, Phys. Rev. B **46**, 1244 (1992), R.P. Singh, M. Singh, Phys. Rev. B **46**, 14069 (1992).
3. B.G. Liu, Phys. Rev. B **41**, 9563 (1990).
4. Ajay, S. Patra, R.S. Tripathi, Phys. Stat. Sol. (b) **188**, 787 (1995).
5. A. Pratap, Ajay, R.S. Tripathi, Phys. Stat. Sol. (b) **197**, 453 (1996).
6. P. Kopietz, Phys. Rev. Lett. **68**, 3480 (1992).
7. A. Auerbach, D.P. Arovas, Phys. Rev. Lett. **61**, 617 (1988).
8. B. Keimer, A. Aharony, A. Auerbach, R.J. Birgeneau, A. Cassanho, Y. Endoh, R.W. Erwin, M.A. Kastner, G. Shirane, Phys. Rev. B **45**, 7430 (1992).
9. J.M. Tranquada, D.E. Cox, W. Kunnmann, H. Moudden, G. Shirane, M. Suenaga, P. Zolliker, D. Vaknin, S.K. Sinha, M.S. Alvarez, A.J. Jacobson, D.C. Johnston, Phys. Rev. Lett. **60**, 156 (1988).
10. J.M. Tranquada, G. Shirane, B. Keimer, S. Shamoto, M. Sato, Phys. Rev. B **40**, 4503 (1989).
11. J.M. Tranquada, P.M. Gehring, G. Shirane, S. Shamoto, M. Sato, Phys. Rev. B **46**, 5561 (1992).
12. S. Shamato, M. Sato, J.M. Tranquada, B.J. Sternlieb, G. Shirane, Phys. Rev. B **48**, 13817 (1993).
13. R. Stern, R. Mall, J. Roos, D. Brinkmann, Phys. Rev. B **52**, 13817 (1995).
14. D. Reznik, P. Bourges, H.F. Fong, L.P. Regnault, J. Bossy, C. Vettier, D. Milius, I.A. Aksay, B. Keimer, Phys. Rev. B **53**, R14741 (1996).
15. A. Pratap, Govind, R.S. Tripathi, Phys. Rev. B **60**, 6775 (1999).
16. A.J. Millis, H. Monien, Phys. Rev. B **54**, 16172 (1996).
17. A.J. Millis, H. Monien, Phys. Rev. B **50**, 16606 (1994).
18. A. Du, G.M. Li, G.Z. Wei, Phys. Stat Sol. (b) **203**, 517 (1997).
19. D.N. Zubarev, Sov. Phys. Usp. **3**, 302 (1960).
20. Govind, A. Pratap, Ajay, R.S. Tripathi, Pramana **54**, 423 (2000).